Participation of DERs to the Bottom-Up Power System Frequency Restoration Processes

Francesco Sanniti, *Member, IEEE*, Roberto Benato, *Senior Member, IEEE*, and Federico Milano, *Fellow, IEEE*

Abstract— This paper studies the transient behavior and frequency stability of a grid with a large share of distributed energy resources (DERs) during a bottom-up restoration process. This work is motivated by a real-world restoration process, during which the tripping of the DER frequency protections led to the frequency instability and finally to the collapse of the system. The main contribution of the paper is the proposal of a DER control strategy based on the estimation of the rate of change of frequency and fast frequency regulation. A comprehensive stochastic analysis in time domain shows that the proposed control effectively prevents the occurrence of the instability during the restoration process.

Index Terms— Power system restoration, Distributed Energy Resource (DER), Rate of Change of Frequency (RoCoF), stochastic differential-algebraic equations.

I. INTRODUCTION

A. Motivation

An emerging challenge of power system restoration is the growing share of Distributed Energy Resources (DERs) in distribution networks. DERs impact on the steady-state security [1], [2] as well as on the transient stability [3], [4] of the restoration process. The traditional bottom-up restoration strategy does not appear to be suitable anymore for networks with high penetration of non-synchronous generation. The dynamic response and protection of DERs, in fact, introduce a high level of volatility in the overall dynamic response of the grid during the restoration process.

The effect of DERs on restoration can be well illustrated with an event occurred in Northern Italy in 2020, when a simultaneous frequency protection tripping of the DER units led to the system collapse during a restoration test. Figure 1 shows the actual recordings of this event. The active power generated by the pilot power plant (blue line) decreases after each portion of the distribution system is restored since the DERs gradually supply the loads. However, the frequency deviation following each step triggered the under-frequency relays of the DERs. This eventually led to the system collapse when the pilot generator under-frequency protection has switched off due to the further power unbalance (see zoomed box corresponding to $t \approx 7000$ s in Fig. 1).

F. Sanniti and R. Benato are with the Department of Industrial Engineering, University of Padova, Italy. (e-mails: francesco.sanniti@phd.unipd.it and roberto.benato.unipd.it).

F. Milano is with the School of Electrical & Electronic Engineering, University College Dublin, Ireland. (e-mail: federico.milano@ucd.ie).
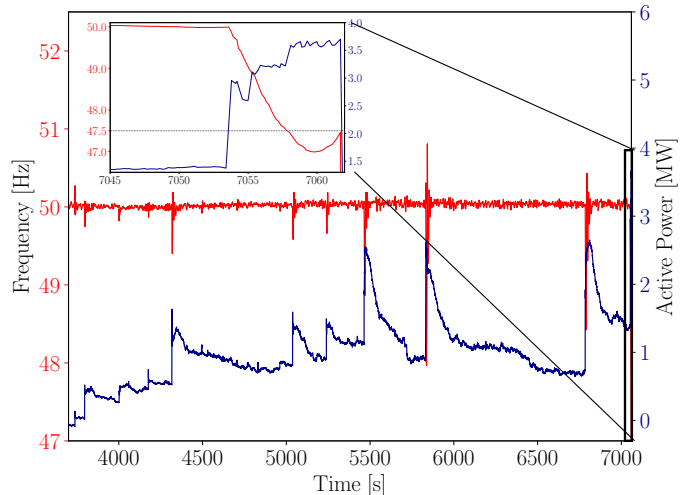
Fig. 1. Frequency (red line) and active power (blue line) measurements of a real-world power system restoration test performed in Northern Italy in 2020.

In this real-world example, the collapse was ultimately caused by the frequency protection systems of the DERs that were set to comply with the requirements of distribution operators, i.e. short circuits faults and anti-islanding issues [5], [6]. These settings, however, do not always fit the needs of the transmission system. During the restoration process, in fact, the bulk power system is characterized by a very low inertia and is thus particularly sensitive to any power unbalance. This paper proposes a simple yet effective control strategy of DERs that, while not compromising the normal operation of the system, is able to prevent the triggering of their protections during the restoration.

B. Literature Review

The research on power system restoration has traditionally focused on system operation issues [7], the main objective being the optimal allocation of resources to restore, maximize the portion of recovered load and minimize the outage time [8], [9]. This is generally formulated as a constrained optimization problem [10]. The stability analysis of the restoration process has become relevant only in last two decades [11]–[13] and has been also studied through mock drills [14], [15], which, however, were based on conventional synchronous-machine dominated power systems. The problem of the system collapse caused by frequency variations have been studied also in the field of the control of microgrids [16], [17]. Moreover, microgrids have been exploited to perform service restoration [18]. Several emerging technologies have been proven to be effective for the bulk power system restoration process,

such as Battery Energy Storage Systems (BESSs) [19], Line-Commutated Converter (LCC)-High Voltage Direct Current (HVDC) transmission systems [20] and Voltage Source Converter (VSC)-HVDC ones [21] .

Very recently, the stability analysis of power system restoration has faced a new challenge due to the ever increasing share of DERs on the distribution side. Several recent works propose to involve the models of distributed resources in the study of the restoration process [3], [4], [22], [23]. References [24] and [25] show that if the DERs provide frequency support through a conventional droop control, the frequency behaviour during the restoration process is improved. However, as we have discussed above, while potentially ameliorating the restoration process in terms of generation capability, the untimely disconnection of DERs can lead to a system collapse.

Only in recent years, international standards have been trying to cope with the DER protection issues. A popular solution consists in *relaxing* the thresholds of the frequency and of the Rate of Change of Frequency (RoCoF) protections [26]. This solution, while avoiding the untimely trigger of the frequency protections during the restoration process, constitutes a potential problem in normal operation. In normal operation, in fact, larger thresholds of the protections may sustain chortcircuit currents or lead to separate portions of the distribution grid. To avoid these events, in [27] a protection with enlarged frequency thresholds but with the ability to shrink the threshold based on a zero sequence voltage detection is implemented.

A more sophisticated solution consists in the implementation of an Active Network Management (ANM) system that remote controls each single DER unit connected to the distribution network. A standard on ANMs has been defined, e.g., in Great Britain [28]. If an ANM is implemented in accordance with the IEC 61850 standard [29], the Distribution System Operator (DSO) can act remotely on the threshold of each DER unit and thus avoid the undesired disconnection of the DERs during a restoration process. However, there are still several DERs that are equipped with standard frequency protections that use conservative (strict) frequency thresholds, making the power system not reliable for the classical restoration process.

C. Contributions

The paper demonstrates how the role of DERs can be converted from passive and potentially harmful "observers" to pro-active "players" of the restoration process after a blackout. The specific contributions are threefold, as follows.

- We propose a model to study the transient behavior and frequency stability of a bottom-up power system restoration considering a large share of DERs and their protection schemes.
- We show that the contribution of a conventional droop control for DER units might not be enough to prevent the system collapse during the restoration process, in case of tripping of DER frequency protections.
- We propose a solution based on a RoCoF control for DERs. This solution is shown to solve the protection tripping issue without compromising the system dynamic performance in normal operation.

The proposed solution is as simple as effective and does not require a specific set up. The effectiveness of the proposed control strategy is thoroughly tested considering a stochastic analysis and under several scenarios. These scenarios take into account the effect of volatility of lags and frequency relays on the restoration process. In particular, we consider stochastic processes to model the load absorption and the amount of DER power disconnected by the frequency relays. Moreover, it is relevant to note that an advatange of the proposed approach is to be based on conventional DER fast frequency control. Using technology that is already commonly included in DERs, in fact, avoids the need for expensive *ad hoc* hardware and communication systems.

D. Paper Organization

The remainder of the paper is organized as follows. Section II outlines the model utilized to simulate the dynamic behavior of the grid during the restoration process. Section III presents the case study, which considers a variety of DER configurations. These include various frequency protection tripping setups and different levels of DER generation capacity. Section IV draws conclusions and outlines future work.

II. MODELLING

Power systems subject to random perturbations and noise can be conveniently modeled as a set of hybrid stochastic differential-algebraic equations and switching diffusions, as follows [30], [31]:

$$
\begin{aligned}
\dot{\boldsymbol{x}} &= \boldsymbol{f}(\boldsymbol{x}, \boldsymbol{y}, \boldsymbol{\eta}, \boldsymbol{u}, \boldsymbol{\alpha}), \\
\boldsymbol{0} &= \boldsymbol{g}(\boldsymbol{x}, \boldsymbol{y}, \boldsymbol{\eta}, \boldsymbol{u}, \boldsymbol{\alpha}), \\
\dot{\boldsymbol{\eta}} &= \boldsymbol{a}(\boldsymbol{\eta}) + \boldsymbol{b}(\boldsymbol{\eta}) \circ \boldsymbol{\xi}, \\
\boldsymbol{0} &= \boldsymbol{h}(\boldsymbol{x}, \boldsymbol{y}, \boldsymbol{\eta}, \boldsymbol{u}) - \boldsymbol{\alpha},
\end{aligned}
\tag{1}
$$

with initial conditions

$$
\begin{aligned}
\boldsymbol{x}(t_o) &= \boldsymbol{x}_o, & \boldsymbol{y}(t_o) &= \boldsymbol{y}_o, & \boldsymbol{\eta}(t_o) &= \boldsymbol{\eta}_o, \\
\boldsymbol{u}(t_o) &= \boldsymbol{u}_o, & \boldsymbol{\alpha}(t_o) &= \boldsymbol{\alpha}_o,
\end{aligned}
\tag{2}
$$

where $\boldsymbol{x} \in \mathbb{R}^l$ is the vector of state variables; $\boldsymbol{y} \in \mathbb{R}^m$ is the vector of algebraic variables; $\boldsymbol{\eta} \in \mathbb{R}^n$ represents the vector of uncorrelated stochastic processes; $\boldsymbol{\xi} \in \mathbb{R}^n$ is a vector of n-dimensional uncorrelated white noise; $\boldsymbol{u} \in \mathbb{R}^r$ represents the vector of input variables (e.g., reference voltage of the voltage controllers and DER active and reactive power set points); and $\boldsymbol{\alpha} \in \mathbb{R}^s$ are continuous-time Markov chains (i.e. discrete events) modelled through finite-state processes. The equations $\boldsymbol{f} : \mathbb{R}^{l+m+n+r+s} \mapsto \mathbb{R}^l$ are the deterministic differential equations; whereas $\boldsymbol{g} : \mathbb{R}^{l+m+n+r+s} \mapsto \mathbb{R}^m$ are the algebraic equations. The stochastic processes feature two terms: the drift, $\boldsymbol{a} : \mathbb{R}^n \mapsto \mathbb{R}^n$, and the diffusion, $\boldsymbol{b} : \mathbb{R}^n \mapsto \mathbb{R}^n$. Equations $\boldsymbol{h} : \mathbb{R}^{l+m+n+r} \mapsto \mathbb{R}^s$ represent the switching diffusions that define the discrete events $\boldsymbol{\alpha}$. Finally, $\circ$ represents the Hadamard product, i.e., the element-by-element product of two vectors.

In the remainder of this work, we assume the following.

- The stochastic processes $\boldsymbol{\eta}$ are additive and are applied to the load power consumption.

- The power set points of the DERs are modelled as a subset of $\boldsymbol{u}$ and are initialized randomly using a uniform distribution at the beginning of each time domain simulation.
- The amount of power of the DERs shed as a consequence of the frequency protection tripping is modelled as the continuous-time discrete events $\boldsymbol{\alpha}$.

The schemes of the DER controllers as well as of the specific equations that describe the stochastic processes are given in the remainder of this section.

A. Black Start Unit Model

The bottom-up restoration process requires a pilot generation unit with low consumption auxiliary services, a fast power supply system and a high inertia. Typically, the most suitable generation units are hydro- or gas-turbine power plants [32]. In this paper, we consider a conventional hydroelectric power plant since this was the unit discussed in the introduction and illustrated with Fig. 1. The Synchronous Generator (SG) is represented with a classical 4th order (two-axes) model [33]. The voltage regulation is provided with a simplified Automatic Voltage Regulator (AVR) IEEE type DC-1 [34]. The frequency control and the turbine model diagram are shown in Fig. 2.
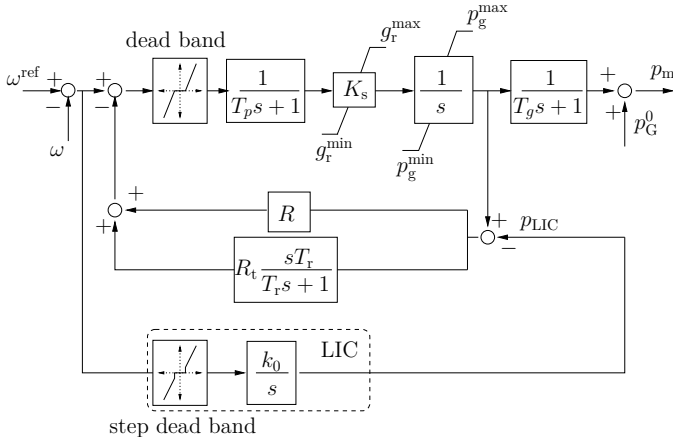

Fig. 2. Frequency control diagram of the black start unit.

For the Primary Frequency Control (PFC) and for the turbine model, we utilize the governor for hydraulic turbines model of [35] and we insert an additional channel to provide Local Integration Control (LIC). The LIC is generally enabled for emergency condition frequency deviations through a step dead-band and is always installed on the black start units. The LIC ensures the perfect tracking of the frequency also for isolated generators without Automatic Generation Control (AGC) [36]. Compared to AGC, however, the LIC is characterized by a higher gain k_0 in order to speed up the frequency restoration.

The effect of the frequency regulator can be related to the power balancing of the system with only one SG through the well-known swing equation:

$$M_G \dot{\omega} = p_m - p_G + D_G \Delta\omega \,, \qquad (3)$$

where $\Delta\omega = \omega^{\text{ref}} - \omega$ is the rotor speed deviation from the reference angular speed ω^{ref}; D_G is the damping; M_G is the

mechanical starting time; p_G is the electrical power of the SG injected into the grid; and p_m is the mechanical power of the SG. The mechanical power can be assumed to be the sum of three components:

$$p_m = p_G^0 + p_{\text{PFC}} + p_{\text{LIC}} \,, \qquad (4)$$

where p_G^0 is the power set point obtained by solving the power flow problem; p_{PFC} is the active power regulated by the PFC and p_{LIC} is the active power regulated by the LIC.

B. DER Model

This section describes the DER aggregated model and controllers that are utilized in all examples of the case study presented in Section III. Note that the utilization of an aggregated model does not reduce the generality of the study carried out in this work as we take into account aspects such as network topology and effects of granularity of the distribution system through the diffusion switching process described below in this section. This stochastic approach allows considering the spatial distribution of the DER units through a temporal effect, by applying a stochastic behaviour on the switching diffusion of the DER aggregation, as outlined below. This modelling appears appropriate as the DERs connected to the distribution system are for the most part small-capacity grid-following devices, which have thus little influence on local frequency fluctuations of the grid [37].

The block diagram of the DER control model is shown in Fig. 3. This model consists of an inner control loop, that regulates the current components i_d and i_q in the dq-axis reference frame, and one outer loop that implements the frequency control. This controller is fed with the angular frequency error $\omega^{\text{ref}} - \omega$ and implements a proportional droop control with constant R_D and a low-pass filter with time constant T_f as well as a RoCoF control with washout filter with time constant T_w. In the case study, for some scenarios, the RoCoF control is disabled by setting $T_w = 0$. The frequency control output is then added to the DER active power reference p_D^{ref}.
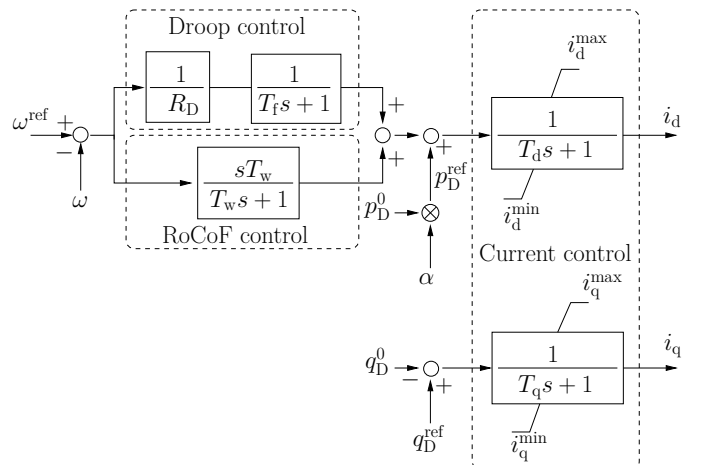

Fig. 3. Diagram of the inner and the outer control loops of the DER model.

The current components i_d and i_q are limited by two anti wind-up limiters, in order to bind the generated power to the maximum capacity of the aggregation of DERs. The active and the reactive power output p_D and q_D of the DER are then obtained from the current components i_d and i_q as follows:

$$
\begin{aligned}
p_\mathrm{D} &= v_\mathrm{d} i_\mathrm{d} + v_\mathrm{q} i_\mathrm{q}, \\
q_\mathrm{D} &= v_\mathrm{q} i_\mathrm{d} - v_\mathrm{d} i_\mathrm{q}.
\end{aligned}
\tag{5}
$$

It is convenient to recall how the controls implemented on DER affect the implementation of the swing equation (3). In the first instants following a contingency, (3) becomes:

$$
(M_\mathrm{G} + T_\mathrm{w})\dot{\omega} = (p_\mathrm{m} + p_\mathrm{D}^\mathrm{ref}) - p_\mathrm{L} + (D_\mathrm{G} + 1/R_\mathrm{D})\Delta\omega, \tag{6}
$$

where p_L is the total electrical power absorbed by the loads and R_D is the constant of the droop control. Equation (6) shows the contribution of the RoCoF control on the total equivalent inertia of the system during the first instants after a contingency.

A frequency relay logic is also implemented to control the DER power reference $p_\mathrm{D}^\mathrm{ref}$ by multiplying the power of the DER in steady state, p_D^0, by a continuous variable $\alpha \in [0, 1]$, hence:

$$
p_\mathrm{D}^\mathrm{ref} = \alpha\, p_\mathrm{D}^0. \tag{7}
$$

This quantity α models the tripping behaviour of an aggregation of DERs and is defined as the product of two components:

$$
\alpha = h_\mathrm{det}\, h_\mathrm{noise}, \tag{8}
$$

where h_det is deterministic and h_noise is a continuous-time Markov chain.

The deterministic component h_det is associated with the frequency protection thresholds imposed by national and/or international standards, e.g. [5], [6], [38], [39], as discussed in Section I. The component h_det is a staircase function with ν steps of generation of size k_i, $i = 1, \ldots, \nu$, with $\sum_{i=1}^{\nu} k_i = 1$. Each generation step *certainly* trips if the frequency deviation exceeds the threshold ε_i, $i = 1, \ldots, \nu$. The overall tripping logic is given by:

$$
h_\mathrm{det} =
\begin{cases}
1, & \text{if } |\Delta\omega| \le \varepsilon_1, \\
1 - k_1, & \text{if } \varepsilon_1 < |\Delta\omega| \le \varepsilon_2, \\
\vdots & \vdots \\
1 - \sum_{i=1}^{j} k_i, & \text{if } \varepsilon_j < |\Delta\omega| \le \varepsilon_{j+1}, \\
\vdots & \vdots \\
1 - \sum_{i=1}^{\nu-1} k_i, & \text{if } \varepsilon_{\nu-1} < |\Delta\omega| \le \varepsilon_\nu, \\
0 = 1 - \sum_{i=1}^{\nu} k_i, & \text{if } |\Delta\omega| > \varepsilon_\nu,
\end{cases}
\tag{9}
$$

where $\Delta\omega = \omega_0 - \omega$ is the angular speed deviation from the nominal speed ω_0. The blue lines in Fig. 4 illustrate (9) for different values of ν.

Equation (9) is suitable to model a given number of clusters of small DERs. However, the behavior of aggregated DER model that includes several smaller devices shows, in practice, a more granular and volatile response. To take into account that aggregated DER models do not trigger their full capacity instantaneously, we include the switching diffusion h_noise. This component has ultimately the effect of making the discrete event α stochastic. The model that defines the continuous Markov chain for each step of generation k_i is as follows.

We assume that each step k_i is composed by sub-steps κ_i^j, for $j = 1, \ldots, \mu$, where κ_i^j are the components of a vector $\boldsymbol{\kappa}_i$ defined as follows:

$$
\boldsymbol{\kappa}_i = k_i \boldsymbol{r}_i, \tag{10}
$$

where $\boldsymbol{r}_i = [r_i^1, \ldots, r_i^j, \ldots, r_i^\mu]$ is a vector with $r_i^j \sim \mathcal{U}[0, 1]$, i.e., the elements r_i^j are uniformly distributed in the range $[0, 1]$ and satisfy the condition:

$$
\sum_{j=1}^{\mu} r_i^j = 1. \tag{11}
$$

The frequency threshold ε_i is also split into randomly distributed sub-intervals $e_i^j \sim \mathcal{U}[\varepsilon_i - \Delta\varepsilon_i, \varepsilon_i + \Delta\varepsilon_i)]$, for $j = 1, \ldots, \mu$, where $\Delta\varepsilon_i$ is the uncertainty on ε_i, and they are sorted in order to satisfy the conditions:

$$
(\varepsilon_i - \Delta\varepsilon_i) \le e_i^1 < e_i^2 < \cdots < e_i^\mu \le (\varepsilon_i + \Delta\varepsilon_i). \tag{12}
$$

Similarly to (9), the switching diffusion h_noise is composed of ν blocks, and each block has μ random steps. The i-th block, say h_noise^i is given by:

$$
h_\mathrm{noise}^i =
\begin{cases}
1, & \text{if } |\Delta\omega| \le e_i^1, \\
1 - r_i^1, & \text{if } e_i^1 < |\Delta\omega| \le e_i^2, \\
\vdots & \vdots \\
1 - \sum_{j=1}^{l} r_i^j, & \text{if } e_i^j < |\Delta\omega| \le e_i^{j+1}, \\
\vdots & \vdots \\
1 - \sum_{j=1}^{\mu-1} r_i^j, & \text{if } e_i^{\mu-1} < |\Delta\omega| \le e_i^\mu, \\
0 = 1 - \sum_{j=1}^{\mu} r_i^j, & \text{if } |\Delta\omega| > e_i^\mu.
\end{cases}
\tag{13}
$$

The red lines in Fig. 4 illustrate the behaviour of the random processes κ_i^j and e_i^j, and Fig. 5 gives a detail of Fig. 4 for the i-th step. Note that for $\mu = 1$, α collapses to the deterministic function h_det (blue lines of Fig. 4 and Fig. 5).

C. Load Model

The load power consumption models represent areas containing several thousands of physical devices and appliances. In this paper, the stochastic behavior of these equivalent aggregated loads, formulated as in [30], is as follows:

$$
\begin{aligned}
p_\mathrm{L} &= p_\mathrm{L0} + \eta_p, \\
q_\mathrm{L} &= q_\mathrm{L0} + \eta_q, \\
\dot{\eta}_p &= -a_p \eta_p + b_p \xi_p, \\
\dot{\eta}_q &= -a_q \eta_q + b_q \xi_q,
\end{aligned}
\tag{14}
$$

where p_L0 and q_L0 represent active and reactive load powers; a_p and a_q are the mean-reversion speed terms; b_p and b_q are used to adjust the variance of the processes; η_p and η_q are two stochastic processes with zero means and standard deviations $b_p/\sqrt{2a_p}$ and $b_q/\sqrt{2a_q}$, respectively; and ξ_p and ξ_q are white noises.
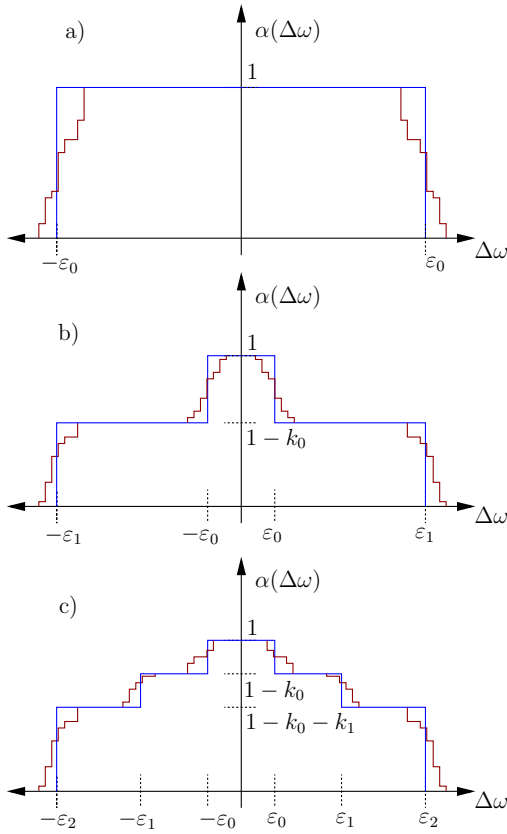
Fig. 4. Graphical representation of the function that defines the discrete event α: (a) $\nu = 0$, (b) $\nu = 1$ and (c) $\nu = 2$; the blue lines represents h_{det} alone ($\mu = 1$), whereas the red lines represent $h_{\text{det}} h_{\text{noise}}$.
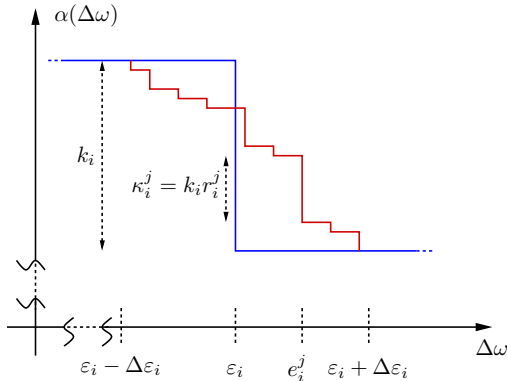

Fig. 5. Graphical representation of the function that defines the discrete event α for the i-th block of generation; the blue lines represents h_{det} alone ($\mu = 1$), whereas the red lines represent $h_{\text{det}} h_{\text{noise}}$.
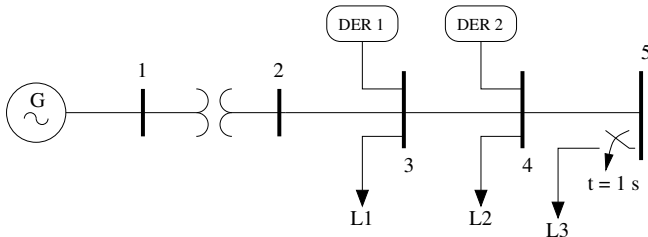

Fig. 6. Test grid utilized in the case study.

III. CASE STUDY

This case study illustrates the impact of DERs connected to the distribution grid on the dynamic performance of a bottom-up power system restoration process. With this purpose, we consider the grid depicted in Fig. 6.

The grid is built *ad hoc* for this study and consists of:

- A hydroelectric power unit equipped with a conventional synchronous generator connected to bus 1;
- A 15/230 kV step-up transformer that connects buses 1 and 2;
- Three 230 kV transmission lines that connect buses from 3 to 5;
- Three aggregated loads connected at buses from 3 to 5 and representing the power consumption of distribution grids;
- Two units of aggregated DERs connected at buses 3 and 4 and representing the distributed generation connected at the distribution grid level. DER1 follows the tripping driven by the switching diffusion α as discussed in Section II-B, and DER2 provides frequency support. In particular, for the deterministic component of α, h_{det}, we assume two main thresholds, namely, $0,006$ pu(Hz) and 0.02 pu(Hz), as these are the values currently utilised by most DERs of the Italian distribution network. The DER units are assumed to generate the maximum power allowable by their prime source. The uncertainty on the DER generation is not taken into account since we are interested in the time scale of few tens of seconds, when the generated power can be assumed to remain constant.

In all scenarios discussed in the remainder of this section, we assume that the hydroelectric power unit energizes buses 1 to 5, and that L1, L2, DER1 and DER2 are connected to the grid. Then, we simulate the connection of load L3 at $t = 1$ s assuming that the system is in steady-state with the operating condition shown in Table I, which was obtained with the grid data given in the Appendix.

TABLE I
INITIAL OPERATING POINT OF THE TEST SYSTEM OF FIG. 6.

Bus	$|\bar{v}|$	$\angle \bar{v}$	$p_{\text{G}}, p_{\text{D}}$	$q_{\text{G}}, q_{\text{D}}$	p_{L}	q_{L}
#	[pu(kV)]	[rad]	[pu(MW)]	[pu(Mvar)]	[pu(MW)]	[pu(Mvar)]
1	1.000	0	-0.2	-0.056	0	0
2	1.005	-0.0194	0	0	0	0
3	1.010	-0.0417	-0.2	-0.03	0.2	0.03
4	1.022	-0.0418	0	0	0.2	0.03
5	1.024	-0.0418	0	0	0	0

The connection of load L3 causes an active power unbalance of $p_{\text{L3}} = 0.089$ pu(MW). This leads to a decrease of the synchronous rotor speed and, hence, of the system frequency. The amount of the power insertion is chosen on purpose. It is, in fact, the minimum power that makes the frequency nadir to reach the value of the under-frequency protection threshold, namely, 0.95 pu(Hz) in this case study. This is a typical value that triggers the majority of the synchronous generators [40].

Then, we assume that loads L1 and L2 are stochastic and described by (14). DER1 power set point is defined by

$\alpha_{\mathrm{D}1}\,p_{\mathrm{D}1}^{0}$, where $\alpha_{\mathrm{D}1}$ is the stochastic variable described in Section II-B. The set point of DER2, on the other hand, is assumed to be always deterministic, i.e., $\alpha_{\mathrm{D}2} = 1$, and to be null in steady state, i.e. $p_{\mathrm{D}2}^{0} = 0$, in order to guarantee a plenty capability reserve to provide under frequency regulation after the power unbalance (its total capacity is 10 MVA).

DER1 and DER2 are modelled as in Fig. 3 and their control capability depends on the scenario, as follows.

- **Scenario 0** (S0): the DERs do not trip and do not provide frequency control (Section III-A).
- **Scenario 1** (S1): the DERs can trip and do not provide frequency control (Section III-B).
- **Scenario 2** (S2): the DERs can trip and provide frequency control (Section III-C).
- **Scenario 3** (S3): the DERs can trip and provide frequency and RoCoF control (Section III-D).
- **Scenario 4** (S4): same as S1 but considering a Monte Carlo analysis and a switching diffusion $\alpha_{\mathrm{D}1}$ in DER1 (Section III-E).
- **Scenario 5** (S5): same as S1, S2 and S3 but considering a Monte Carlo analysis with uniformly distributed initial power set point of the DERs (Section III-F).

Section III-G performs a comparison between the proposed solution and other possible solutions proposed in the literature. The data of the grid as well as the parameters of the synchronous machine, of the loads and of the DER are given in the Appendix. Simulations are carried out with the Python-based software tool Dome [41].

A. Scenario 0

This scenario assumes that the DER units do not switch off and do not provide frequency support. In this scenario, thus, $\alpha_{\mathrm{D}1}$ has the shape shown in Fig. 4a with the parameters of the second column of Table IX. The results of this simulation are shown in Fig. 7. As expected, the frequency nadir reaches the minimum value of 0.95 pu(MW), the restoration process completes successfully and the system remains stable.

It is important to note that this scenario represents, in turn, the behavior of the "conventional" grid, i.e., the distribution system including only passive loads. The fact that the system is stable indicates that the instabilities shown in S1 and S2 are due to the protections and the ineffective control of the DERs.

B. Scenario 1

In this scenario, the DERs can trip and do not provide frequency control. As discussed in Section I, it is reasonable to assume that, in some networks, a non negligible quota of DERs may still utilize a strict frequency threshold.

With this in mind, in this scenario, two frequency protection setups are considered. The first setup (S1a) assumes that the half of the DER1, corresponding to half of the generated power (0.1 pu(MW)) has one strict frequency protection threshold. For S1a, the shape of $\alpha_{\mathrm{D}1}$ is the one shown in Fig. 4b with the parameters of the third column of Table IX. The second setup (S1b) assumes that the same amount of DER1 (0.1 pu(MW)) has two strict frequency protection thresholds. For S1b, thus,
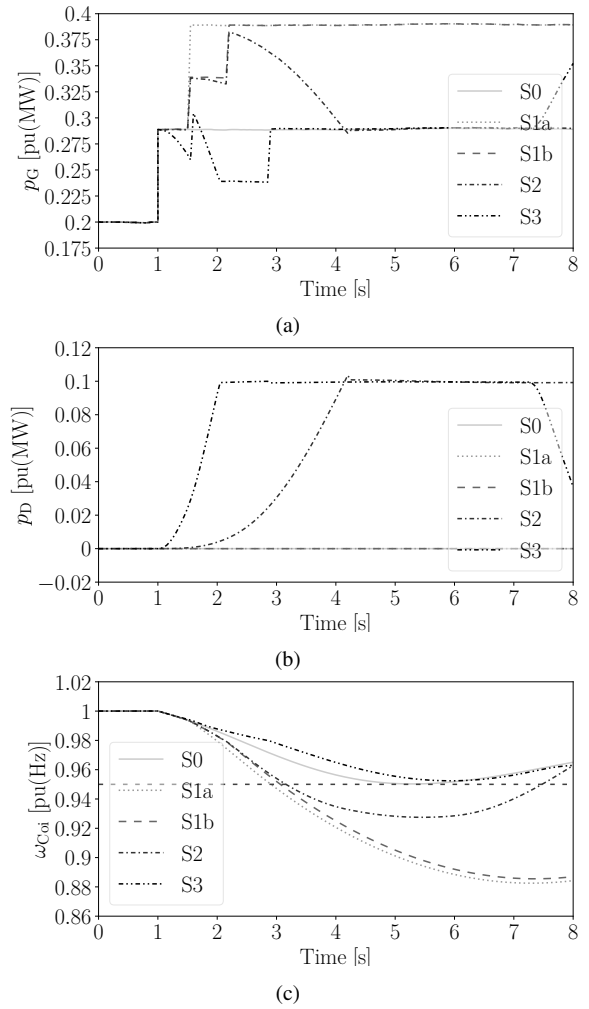

Fig. 7. Simulation results for scenarios S0-S3: (a) active power generated by the hydroelectric black start unit; (b) active power generated by DERs; and (c) frequency of the CoI.

the shape of $\alpha_{\mathrm{D}1}$ is the one shown in Fig. 4c with parameters of the fourth column of Table IX.

Simulation results for these scenarios are shown in Fig. 7. The early tripping of the DER frequency protections makes the frequency to exceed the threshold of the hydroelectric generator, due to the higher amount of load which has to be balanced. The system eventually collapses as a consequence of the trip of the black start unit. This happens both for S1a and S1b, thus indicating that relaxed frequency thresholds might be dangerous for the stability of the restoration process.

C. Scenario 2

In this scenario, we discuss the effect of the frequency droop control implemented on the DERs. With this aim, DER2 is assumed to regulate the frequency and the variable $\alpha_{\mathrm{D}1}$ takes the shape shown in Fig. 4c with the parameters of the fourth column of Table IX.

The simulation results of this scenario are shown in Fig. 7. The contribution of the droop control of the DERs enhances, as expected, the frequency behaviour as compared to S1. Nevertheless, the support provided by the DERs is still not enough to avoid the collapse of the system.

D. Scenario 3

In this scenario, we discuss the combined effect of the droop control and of the RoCoF (inertial) control provided by the DERs. The function α_{D1} is assumed to have the shape shown in Fig. 4c with the parameters of the fourth column of Table IX.

Simulation results are shown in Fig. 7. The contribution of the RoCoF control significantly enhances the dynamic response of the system and prevents the system from collapsing. As it appears, the first instants after the connection of L3 are critical for the remaining part of the transient. In fact, the power injected because of the RoCoF control in the first instants following the power unbalance helps reduce the frequency nadir and, hence, prevents the triggering of the DER protections. On the other hand, in the first instants, the conventional droop control of the DERs gives a relatively small contribution, even if in the long term dynamics it is the same of the combined controls.

Note that the same DER frequency response obtained in S3 can also be achieved by applying a smaller value of R_D to the droop control. This specific case is discussed in Section III-G.

E. Scenario 4

In this scenario, α_{D1} is modelled as a stochastic switching diffusion by taking into account different values of frequency protection thresholds, as described in Section II. In particular, α_{D1} is assumed to have the shape shown in Fig. 4c (red lines) and the parameters of the fifth column of Table IX. A Monte Carlo analysis consisting of 250 parallel simulations is carried out. Simulation results are shown in Fig. 8 and indicate that the volatility of the frequency protection of the DERs has a negligible impact on the overall frequency response of the grid. The frequency standard deviation is, in fact, 0.005 pu(Hz).

F. Scenario 5

In this fifth and last scenario, the power share of DERs installed on the distribution grid is varied using a uniform distribution. That is, $p_D^0 \sim \mathcal{U}(0, 0.2)$ pu(MW).

This analysis is applied to S1, S2 and S3. Simulations results are shown in Fig. 9. Figure 9b indicates that the application of the droop control alone is unable to avoid the occurrence of instability for any value of the DER power production. Figure 9c, on the other hand, shows how the RoCoF control prevents from the system collapse for every value of p_D^0. Figure 9c shows two clusters: cluster #1 is related to high values of p_D^0 for which the RoCoF action prevents from the tripping of the second strict threshold (frequency stays above 0.98 [pu]); and cluster #2 is related to lower values of p_D^0. The nonlinear behaviour of the trajectories of the generated powers after the event are related to DER maximum power saturation.

G. Comparison with Other Methods

Table II summarises advantages and drawbacks of the various approaches discussed the literature review (see Section I-B) as well as the approach proposed in this work. Approaches
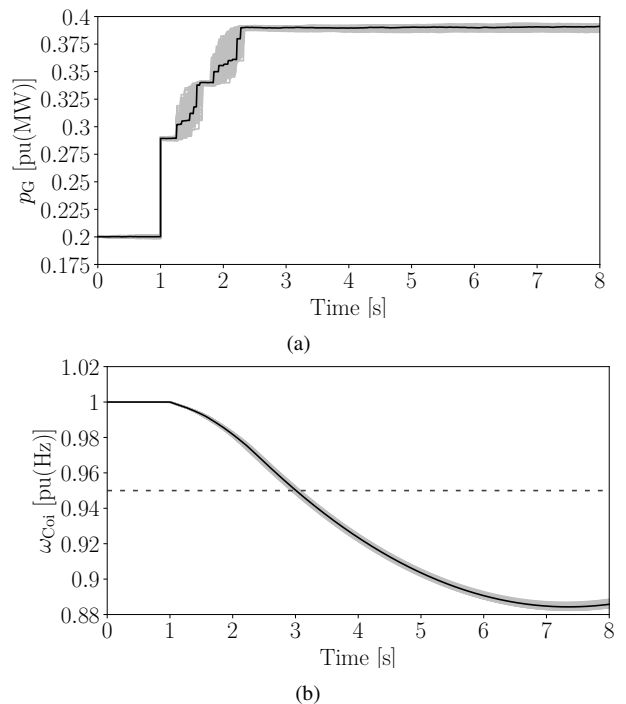

Fig. 8. Results of the 250 realizations for the switching diffusion α_{D1}: (a) active power of the hydroelectric black start unit; and (b) frequency of the CoI.

TABLE II

COMPARISON BETWEEN DIFFERENT SOLUTIONS

#	Solution	Ref.	Pros	Cons
1	Enlarge frequency threshold	[26]	Guaranteed to prevent from triggering	Problems in normal operation: faults and islanding
2	Zero-sequence voltage-based frequency protection	[27]	Guaranteed to prevent from triggering	Need to install new protection
3	ANM	[28]	Remote control on DER protection	Need to build a remote communication system
4	DER with smaller droop constant R_D	This work	Improve the frequency behaviour	Potentially unstable in normal operations
5	DER with RoCoF control	This work	Improve the frequency behaviour	Fast and easy implementation

1 to 3 suggest to prevent from the system collapse eventually by enlarging the thresholds to avoid their trigger during the restoration process. This occurrence lies with the simulation of S0. Approach 4, on the other hand, is implicitly taken into account in S3. In fact, the DER frequency response observed in the results of S3 shown in Fig. 7.b can be also achieved by applying a smaller value of R_D to the droop control. However, reducing the value of the droop is not recommended since small droop values can lead to instability in normal operation. Approach 5 is proposed in this paper and prevents the system from collapsing with no repercussion on the normal operation.

It is relevant to further discuss approach 4 and show why it can lead to instability during normal operation. With this purpose, the well-known WSCC 9-bus system shown in Figure 10 is considered. Base-case data of this benchamrk system are given in [42]. A DER unit is included at Bus 5, using the parameters listed in the Appendix and with a power capacity of 1 [pu]. A small disturbance is applied to Bus 5 at $t = 1$ s.
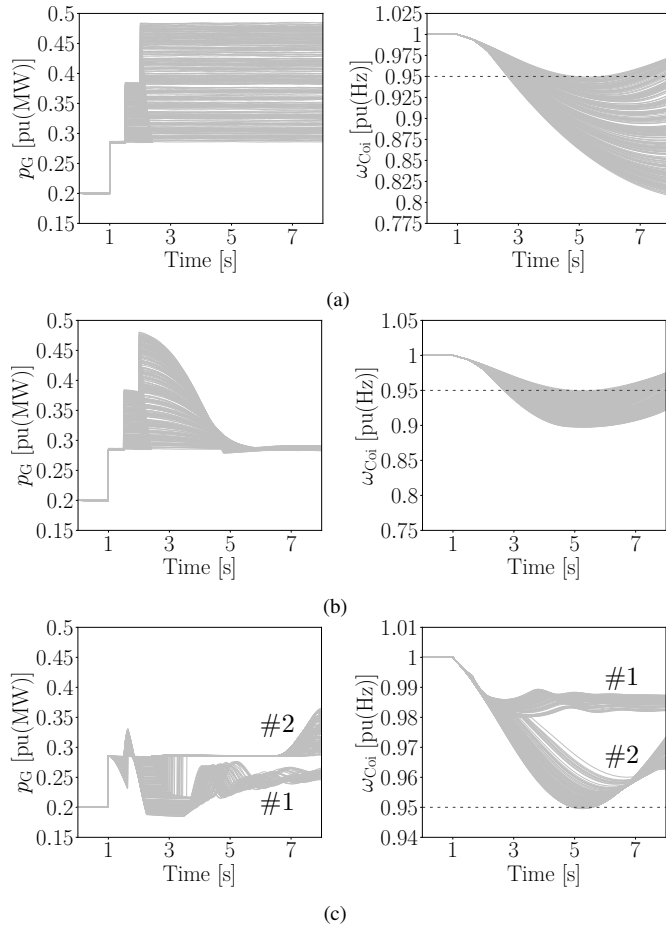
Fig. 9. Results of the Monte Carlo analysis obtained by varying the value of p_D^0: (a) without DER frequency regulation; (b) with DER droop control; (c) with DER droop and RoCoF controls.
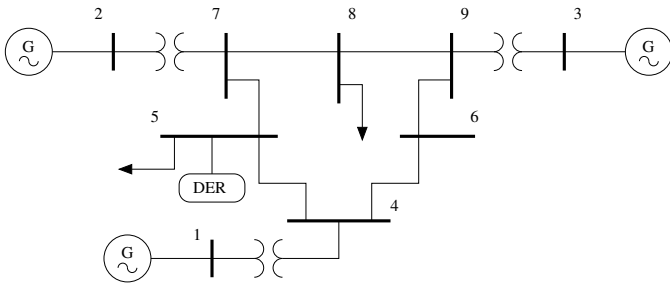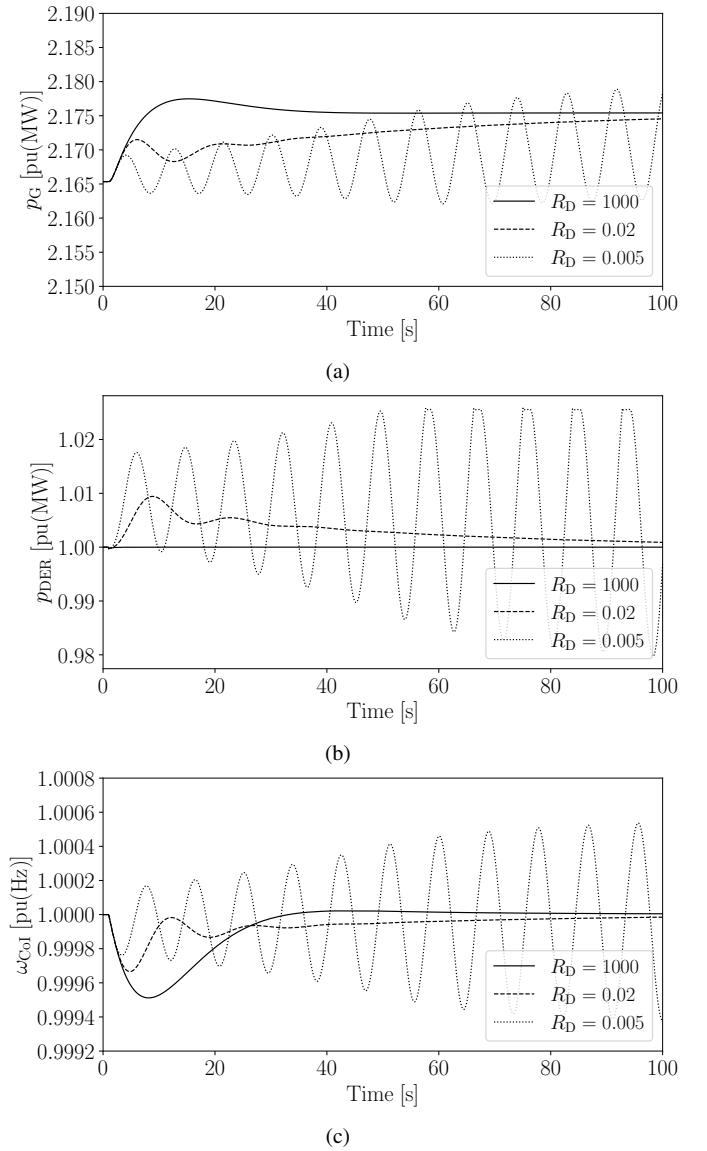

Fig. 10. WSCC 9-bus system.

Fig. 11. Results of the simulation for a small disturbance on the WSCC 9-bus system during normal operation: (a) sum of the turbine power provided by synchronous units; (b) active power provided by DER unit; (c) frequency of the CoI.

IV. CONCLUSIONS

This paper discusses the restoration process from the system dynamic stability point of view considering a high penetration of DERs connected at the distribution network level. The effect of both frequency protection tripping and frequency regulation of aggregated DER models is studied. The impact of load noise, of the volatility of frequency protection thresholds and of the amount of DER capacity is also duly taken into account through detailed stochastic models and Monte Carlo simulations.

The results discussed in the case study indicate that the contribution of a conventional droop control is not sufficient to prevent the system from collapsing following the untimely trip of DER protections. With this aim, we propose a solution based on the implementation of RoCoF-based fast frequency regulation of the DERs. This control is effective as it forces

Figure 11 shows the results of the time domain simulation for different value of R_D. Figure 11.a shows the power generation of the synchronous generators and of the DER, where as Fig. 11.b shows the frequency of the Center of Inertia (CoI) of the system. For $R_D = 1000$, as expected, the contribution of the DER unit is null. For $R_D = 0.02$, which is a typical value for the droop constant of the DER units, first the DER contribution supports the regulation provided by the synchronous units and then is zeroed by the AGC control. Instead, for lower values of R_D, e.g. for $R_D = 0.005$, the system becomes unstable and the electromechanical oscillations diverge.

the DERs to generate more power in the first instants after the occurrence of the power unbalance. The RoCoF control also appears not to have a negative effect on frequency relays and does not compromise the system stability during the normal operation. The first instants after the load restoration step are critical. In the first instants, in fact, the droop control gives a small contribution, but the combination of the two controls significantly reduces the initial frequency deviations and, ultimately, prevents the frequency nadir to go below the thresholds of the DER frequency protections.

The implementation of the proposed type of regulation requires that the DER units must have an adequate capacity reserve and their current limits should not be binding in the initial part of the transient following the power unbalance. Moreover, appropriate standardization for the dynamic response and control of the DERs to fit the restoration process appears necessary. Future work will consider these aspects and elaborate on the impact of ESS (Energy Storage System) to achieve the required inertial response of the DERs.

APPENDIX
GRID DATA

This appendix provides the parameters and the grid data of the restoration backbone depicted in Fig. 6. The power base is 100 MW.

TABLE III

PARAMETERS OF THE PILOT POWER PLANT SYNCHRONOUS GENERATOR.

par. [unit]	description	G
V [kV]	terminal voltage	15
s [pu(MVA)]	power rate	0.75
f_{n} [Hz]	frequency rate	50
M [s]	mechanical starting time	10
$T_{d0}^{'}$ [s]	d-axis transient time constant	9.5
$T_{q0}^{'}$ [s]	d-axis transient time constant	0
r_{a} [pu(Ω)]	armature resistance	0.0021
x_{d} [pu(Ω)]	d-axis synchronous reactance	1.11
$x_{d}^{'}$ [pu(Ω)]	d-axis transient reactance	0.41
x_{l} [pu(Ω)]	leakage reactance	0.172
x_{q} [pu(Ω)]	q-axis synchronous reactance	0.8
$x_{q}^{'}$ [pu(Ω)]	q-axis transient reactance	0.8

TABLE IV

LINE AND TRANSFORMER PARAMETERS.

par. [unit]	description	trasf. 1-2	line 2-3	line 3-4	line 4-5
V_{n} [kV]	primary voltage	15	230	230	230
V_{n2} [kV]	secondary voltage	230	-	-	-
l [km]	line length	-	15	30	20
b [μS/km]	shunt susceptance	0	2.7	2.7	2.7
r [pu(Ω)]	series resistance	0.0027	0.166	0.333	0.222
x [pu(Ω)]	series reactance	0.097	3.17	6.35	4.23

TABLE V

PARAMETERS OF THE PILOT POWER PLANT AVR.

par. [unit]	description	G
A_{e} [−]	1st ceiling coefficient	0.0039
B_{e} [−]	2st ceiling coefficient	0.9
K_{a} [−]	amplifier gain	20
K_{f} [−]	stabilizer gain	0.063
T_{a} [s]	amplifier time constant	0.2
T_{e} [s]	field circuit time constant	0.314
T_{f} [s]	stabilizer time constant	0.35
v_{c}^{max} [pu(kV)]	max regulator voltage	5
v_{c}^{min} [pu(kV)]	min regulator voltage	-5

TABLE VI

PARAMETERS OF THE PILOT POWER PLANT FREQUENCY CONTROL.

par. [unit]	description	G
K_{s} [−]	gate servo gain	5
R [pu(MW)]	permanent droop	0.04
R_{t} [−]	transient droop	0.25
T_{g} [s]	gate power servo time constant	0.2
T_{p} [s]	pilot servo time constant	0.04
T_{r} [s]	reset time	9.2
db [pu(Hz)]	pilot servo dead band	0.0002
g_{r}^{max} [pu(MW/s)]	max rate of change of gate pos.	0.07
g_{r}^{min} [pu(MW/s)]	min rate of change of gate pos.	-0.15
p_{g}^{max} [pu(MW)]	max gate opening	1
p_{g}^{min} [pu(MW)]	min gate opening	0
ω^{ref} [pu(Hz)]	reference rotor speed	1
db_{LIC} [pu(Hz)]	LIC step dead band	0.006
k_{0} [−]	gain of the LIC integrator	0.7

TABLE VII

DETERMINISTIC AND STOCHASTIC PARAMETERS OF THE LOADS.

par [unit].	description	L1	L2	L3
p [pu(MW)]	active power	0.2	0.2	0.089
q [pu(Mvar)]	reactive power	0.03	0.03	0.0089
V [kV]	terminal voltage	230	230	230
$r_{p,q}$ [0, 1]	correlation of p and q	0	0	-
σ_{p} [%(MW)]	standard deviation on p	0.5	0.5	-
σ_{q} [%(MW)]	standard deviation on q	0.5	0.5	-
v_{p} [pu/s]	speed of mean-rev. of p	0.1	0.1	-
v_{q} [pu/s]	speed of mean-rev. of q	0.1	0.1	-

TABLE VIII

PARAMETERS OF THE DERs.

par. [unit]	description	DER1	DER2
S_{n} [MVA]	power capacity	20	10
V [kV]	terminal voltage	230	230
R_{D} [pu(MW)]	droop constant	∞	0.02
T_{f} [s]	t.c. of the droop control	5	5
T_{w} [s]	t.c. of the washout filter	0	1
i_{p}^{max}/i_{p}^{min} [pu(kA)]	max/min d-axis current	1/-1	1/-1
i_{q}^{max}/i_{q}^{min} [pu(kA)]	max/min q-axis current	1/-1	1/-1
T_{d} [s]	t.c. of the d-axis control	1	1
T_{q} [s]	t.c. of the q-axis control	1	1

TABLE IX
PARAMETERS OF THE SWITCHING DIFFUSION α_{D1}.

var.	S0	S1a	S1b-S2-S3	S4	S5
$\nu\,[-]$	0	1	2	2	2
$\mu\,[-]$	–	–	–	7	–
ε_0 [pu(Hz)]	0.05	0.006	0.006	0.006	0.006
k_0 [0, 1]	1	0.5	0.25	0.25	0.25
ε_1 [pu(Hz)]	–	0.05	0.02	0.02	0.02
k_1 [0, 1]	–	0.5	0.25	0.25	0.25
ε_2 [pu(Hz)]	–	–	0.05	0.05	0.05
k_2 [0, 1]	–	–	0.5	0.5	0.5
$\Delta\varepsilon_0$ [pu(Hz)]	–	–	–	0.0012	–
$\Delta\varepsilon_1$ [pu(Hz)]	–	–	–	0.004	–

REFERENCES

[1] R. Roofegari Nejad, W. Sun, and A. Golshani, "Distributed restoration for integrated transmission and distribution systems with DERs," *IEEE Trans. on Power Systems*, vol. 34, no. 6, pp. 4964–4973, 2019.

[2] J. Sprooten, T. Gunst, C. Mestdag, and O. Bronckart, "Power system restoration with high penetration level of renewable generation — new challenges and strategies," in *2014 Saudi Arabia Smart Grid Conference (SASG)*, 2014, pp. 1–8.

[3] C. Hachmann, H. Becker, J. Haack, and M. Braun, "Improving the resilience of power system operation - contribution of renewable energies in power system restoration," in *NEIS 2019; Conference on Sustainable Energy Supply and Energy Storage Systems*, 2019, pp. 1–6.

[4] M. Braun, J. Brombach, C. Hachmann, D. Lafferte, A. Klingmann, W. Heckmann, F. Welck, D. Lohmeier, and H. Becker, "The future of power system restoration: Using distributed energy resources as a force to get back online," *IEEE Power and Energy Magazine*, vol. 16, no. 6, pp. 30–41, 2018.

[5] IEEE Std 1547-2003, "IEEE standard for interconnection and interoperability of distributed energy resources with associated electric power systems interfaces," 2003.

[6] VDE-AR-N 4105:2022-08, "Power generation systems connected to the low-voltage distribution network," 2011.

[7] Y. Liu, R. Fan, and V. Terzija, "Power system restoration: A literature review from 2006 to 2016," *Journal of Modern Power Systems and Clean Energy*, vol. 4, no. 3, pp. 332–341, 2016.

[8] G. Patsakis, D. Rajan, I. Aravena, J. Rios, and S. Oren, "Optimal black start allocation for power system restoration," *IEEE Trans. on Power Systems*, vol. 33, no. 6, pp. 6766–6776, 2018.

[9] S. Liu, R. Podmore, and Y. Hou, "System restoration navigator: A decision support tool for system restoration," in *IEEE PES General Meeting*, 2012, pp. 1–5.

[10] W. Sun, C.-C. Liu, and L. Zhang, "Optimal generator start-up strategy for bulk power system restoration," *IEEE Trans. on Power Systems*, vol. 26, no. 3, pp. 1357–1366, 2011.

[11] M. M. Adibi, *Field Experiences in Reenergization of Electrical Networks from Thermal and Hydro Units.* Wiley-IEEE Press, 2000, pp. 354–360.

[12] ——, "Special consideration in power system restoration. the second working group report," *IEEE Trans. on Power Systems*, vol. 9, no. 1, pp. 15–21, 1994.

[13] M. M. Adibi, J. N. Borkoski, R. J. Kafka, and T. L. Volkmann, "Frequency response of prime movers during restoration," *IEEE Trans. on Power Systems*, vol. 14, no. 2, pp. 751–756, 1999.

[14] B. Delfino, G. Denegri, M. Invernizzi, A. Morini, E. Cima Bonini, R. Marconato, and P. Scarpellini, "Black-start and restoration of a part of the Italian HV network: modelling and simulation of a field test," *IEEE Trans. on Power Systems*, vol. 11, no. 3, pp. 1371–1379, 1996.

[15] M. Sforna and V. C. Bertanza, "Restoration testing and training in Italian ISO," *IEEE Trans. on Power Systems*, vol. 17, no. 4, pp. 1258–1264, 2002.

[16] C. Wang, C. Grebogi, and M. S. Baptista, "Control and prediction for blackouts caused by frequency collapse in smart grids," *Chaos: An Interdisciplinary Journal of Nonlinear Science*, vol. 26, no. 9, 2016.

[17] M. C. Pulcherio, A. A. Renjit, M. S. Illindala, A. S. Khalsa, J. H. Eto, D. A. Klapp, and R. H. Lasseter, "Evaluation of control methods to prevent collapse of a mixed-source microgrid," *IEEE Transactions on Industry Applications*, vol. 52, no. 6, pp. 4566–4576, 2016.

[18] C. L. Moreira, F. O. Resende, and J. A. P. Lopes, "Using low voltage microgrids for service restoration," *IEEE Transactions on Power Systems*, vol. 22, no. 1, pp. 395–403, 2007.

[19] W. Liu, L. Sun, Z. Lin, F. Wen, and Y. Xue, "Multi-objective restoration optimisation of power systems with battery energy storage systems," *IET Generation, Transmission & Distribution*, vol. 10, no. 7, pp. 1749–1757, 2016.

[20] X. Li, C. Liu, and Y. Lou, "Start-up and recovery method with LCC–HVDC systems participation during AC/DC system black-starts," *IET Generation, Transmission & Distribution*, vol. 14, no. 3, pp. 362–367, 2020.

[21] M. Bahrman and P.-E. Bjorklund, "The New Black Start: System Restoration with Help from Voltage-Sourced Converters," *IEEE Power and Energy Magazine*, vol. 12, no. 1, pp. 44–53, Jan. 2014.

[22] R. Benato, G. Bruno, S. D. Sessa, G. M. Giannuzzi, L. Ortolano, G. Pedrazzoli, M. Poli, F. Sanniti, and R. Zaottini, "A novel modeling for assessing frequency behavior during a hydro-to-thermal plant black start restoration test," *IEEE Access*, vol. 7, pp. 47 317–47 328, 2019.

[23] G. Lammert, A. Klingmann, C. Hachmann, D. Lafferte, H. Becker, T. Paschedag, W. Heckmann, and M. Braun, "Modelling of active distribution networks for power system restoration studies," *IFAC-PapersOnLine*, vol. 51, no. 28, pp. 558–563, 2018.

[24] D. Lafferte, A. Klingmann, D. Fetzer, G. Lammert, C. Hachmann, T. Paschedag, and M. Braun, "Black start and island operation of distribution grids with significant penetration of renewable resources," in *Large-Scale Grid Integration of Renewable Energy in India*, New Delhi, India, 2017, pp. 1–6.

[25] C. Hachmann, G. Lammert, D. Lafferte, and M. Braun, "Power system restoration and operation of island grids with frequency dependent active power control of distributed generation," in *NEIS 2017; Conference on Sustainable Energy Supply and Energy Storage Systems*, 2017, pp. 1–6.

[26] IEEE Std 1547-2018, "IEEE standard for interconnection and interoperability of distributed energy resources with associated electric power systems interfaces, (Revision of IEEE Std 1547-2003)," pp. 1–138, 2018.

[27] Terna S.p.a, "Allegato A70: Regolazione Tecnica dei Requisiti di Sistema della Generazione Distribuita," 2012.

[28] EDS 08-5060, "Active network management – Flexible connections," 2020.

[29] IEC 61850-7-420, "Communications systems for distributed energy resources - logical nodes," 2009.

[30] F. Milano and R. Zárate-Miñano, "A systematic method to model power systems as stochastic differential algebraic equations," *IEEE Trans. on Power Systems*, vol. 28, no. 4, pp. 4537–4544, 2013.

[31] G. George Yin and Chao Zhu, *Hybrid Switching Diffusions – Properties and Applications.* New York, NY: Sprnger Science, 2010.

[32] M. M. Adibi, *Power System Restoration: Methodologies & Implementation Strategies.* Hoboken, NJ: John Wiley & Sons, 2000.

[33] F. Milano, *Power System Modelling and Scripting.* London: Springer, 2010.

[34] IEEE Std 421.5-2016, "IEEE recommended practice for excitation system models for power system stability studies, (Revision of IEEE Std 421.5-2005)," pp. 1–207, 2016.

[35] P. Kundur, *Power System Stability and Control.* New York, NY: Mc-Grall Hill, 1994.

[36] H. B. Roos, N. Zhu, J. Giri, and B. Kindel, "An AGC implementation for system islanding and restoration conditions," *IEEE Trans. on Power Systems*, vol. 9, no. 3, pp. 1399–1410, 1994.

[37] F. Milano and Á. Ortega, "A method for evaluating frequency regulation in an electrical grid – Part I: Theory," *IEEE Transactions on Power Systems*, vol. 36, no. 1, pp. 183–193, 2021.

[38] Enel DK-5740, "Criteri di allacciamento di impianti di produzione alla rete MT del distributore," 2007.

[39] Autorità per l'energia elettrica e il gas 84/2012/R/EEL, "Interventi urgenti relativi agli impianti di produzione dell'energia elettrica, con particolare riferimento alla generazione distribuita, per garantire la sicurezza del sistema elettrico nazionale," 2012.

[40] IEEE PC37.106/D10.0, "IEEE draft guide for abnormal frequency protection for power generating plants," pp. 1–50, 2021.

[41] F. Milano, "A Python-based software tool for power system analysis," in *IEEE PES General Meeting*, 2013, pp. 1–5.

[42] P. Sauer and M. Pai, *Power System Dynamics and Stability.* Upper Saddle River, NJ: Prentice Hall, 1998.

Francesco Sanniti (M '19) was born in Feltre, Italy, in 1994. He received the Dr.Ing. Degree in electrical engineering from the University of Padova, Italy, in 2019. Since September 2019, he is a PhD student attending the Post-Graduate Course in Industrial Engineering at the University of Padova. He is currently a visiting PhD student at University College Dublin, Ireland. His main fields of research are dynamic stability and control of power system restoration processes and of low-inertia systems. He is a young member of both CIGRÉ and AEIT.

Federico Milano (F'16) received from the Univ. of Genoa, Italy, the ME and Ph.D. in Electrical Eng. in 1999 and 2003, respectively. From 2001 to 2002 he was with the Univ. of Waterloo, Canada, as a Visiting Scholar. From 2003 to 2013, he was with the Univ. of Castilla-La Mancha, Spain. In 2013, he joined the Univ. College Dublin, Ireland, where he is currently Prof. of Power Systems Control and Protections and Head of Elec. Eng. His research interests include power system modeling, control and stability analysis.

Roeberto Benato (M'02-SM'17) was born in Venezia, Italy, in 1970. He received the Dr.Ing. Degree in electrical engineering from the University of Padova in 1995 and Ph.D. in Power Systems Analysis in 1999. In 2021 he was appointed as Full Professor at the Department of Industrial Engineering at Padova University. He is author of 200 papers and 4 books, edited by Springer, Wolters Kluwer and China Machine Press. He has been member of 6 CIGRÉ Working Groups (WGs) and secretary of 2 Joint WGs, and member of IEEE PES Substations Committee. In 2014 he has been nominated Member of IEC TC 120 "Electrical Energy Storage (EES) Systems" in the WG 4 "Environmental issues of EES systems." Currently, he is also corresponding member of CIGRÉ WG B1.72 "Cable rating verification 2nd part." In 2018 R. Benato has been elevated to the grade of CIGRÉ distinguished member. He is a member of the Italian AEIT.